Colloids and Surfaces A: Physicochemical and Engineering Aspects, 82 (1994) 205–215
0927-7757/94/$07.00

Magnetic resonance studies of intercalated, two-dimensional transition metal chalcogenophosphate lattices[α]

S.P. Sibley[a], A.H. Francis[a,*], E. Lifshitz[b], René Clément[c]

[a]*Department of Chemistry, Univesity of Michigan, Ann Arbor, MI 48109, USA*
[b]*Chemistry Department and Solid State Institute, Technion, Haifa 32000, Israel*
[c]*Laboratoire de Chimie Inorganique, C.N.R.S. U.R.A. 420, Université Paris Sud, 91405 Orsay Cedex, France*

(Received 26 June 1992; accepted 4 August 1993)

Abstract

Transition metal chalcogenophosphates with the formula $M_2P_2X_6$ (where M is a divalent transition metal and X = S, Se) form a family of compounds with layered structures that offer chemically accessible interlamellar spaces and the ability, unique among metal chalcogenides, to intercalate cations via an exchange mechanism. Electron paramagnetic resonance (EPR) spectroscopy was employed to study the exchange of lattice metal ions with intercalate ions and to examine the dynamic behaviour of the solvent–intercalate complex, as well as the coordination geometry and oxidation state of various intercalate cations. Both EPR and optically detected magnetic resonance (ODMR) spectroscopy were used to characterize lattice vacancies arising from displacement of the metal cations from their regular positions to interstitial spaces.

Key words: Intercalate cations; Magnetic resonance; Transition metal chalcogenophosphates; Two-dimensional lattices

Introduction

Transition metal chalcogenophosphates with the formula $M_2P_2S_6$ (where M is a transition metal and X = S, Se) have been studied for many years because of their highly anisotropic physical properties, their unusual solid state chemistry [1,2] and their photoelectrochemistry [3]. The chalcogen atoms in these materials are arranged in close-packed layers. The $M_2P_2X_6$ phases are formed by filling all the octahedral holes between alternate chalcogen layers with M atoms and P_2 pairs in the ratio 2 to 1. The structure, illustrated in Fig. 1, has only weak van der Waals forces between the adjacent chalcogen layers [4]. The direction normal to the layers is designated c^* throughout the following text and the extended, two-dimensional interstitial space between chalcogen planes is referred to as the van der Waals gap (vWG).

Although the $M_2P_2X_6$ phases are structurally similar to the layered transition metal dichalcogenides, their properties are considerably different. The lower oxidation state of the metal in $M_2P_2S_6$ materials (2+) results in a considerably more labile metal cation and the solids exhibit a substantially different solid state chemistry. One of the most intriguing properties of these materials is their ability, unique among metal chalcogenides, to intercalate cations via an exchange mechanism. It is possible to conduct cation exchange reactions with single crystals of these materials and interchange a large percentage of the metal with a

*Corresponding author.
[α]Presented at the 6th International Symposium on Magnetic Resonance in Colloid and Interface Science, Florence, Italy, 22–26 June, 1992.

SSDI 0927-7757(93)02622-L

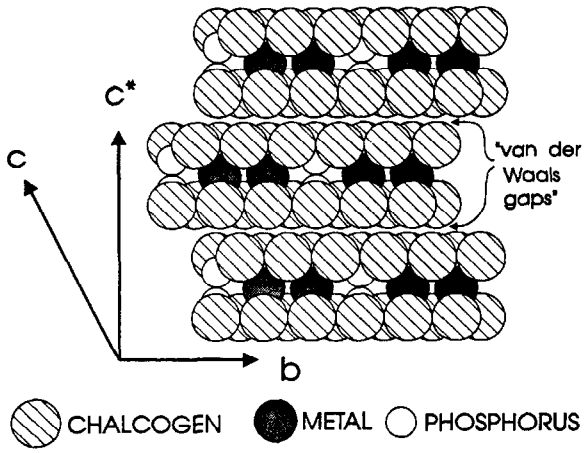

Fig. 1. Schematic structure of $M_2P_2X_6$ materials.

variety of metal, organic and organometallic cations.

The cation exchange process in crystalline $M_2P_2S_6$ lattices involves the replacement of lattice cations by intercalate cations (I^{n+}) when the crystalline solid is in contact with a solution containing the intercalate cations [5]. The exchange process involves a heterogeneous equilibrium between solvated cations in aqueous solution $(I^{n+})_{aq}$ and lattice-coordinated cations in the crystal (M^{2+}). It may be represented as

$$M_2P_2S_6(c) + 2x/nI^{n+}(aq) \leftrightarrow M_{(2-x)}I_{2x/n}P_2S_6(c) + xM^{2+}(aq)$$

Lattice cations have been exchanged at room temperature with intercalate cations having $n = 1, 2, 3$. Clement et al. [6] studied the exchange process by systematically exchanging the lattice cation in several of the $M_2P_2S_6$ lattices with K^+ according to the reaction

$$M_2P_2S_6(c) + 2xK^+(aq) \leftrightarrow M_{2-x}K_{2x}P_2S_6(c) + xM^{2+}(aq)$$

The intercalated potassium cations could be subsequently exchanged with transition metal cations according to the reaction

$$M_{(2-x)}K_{2x}P_2S_6(c) + xI^{2+}(aq) \leftrightarrow M_{(2-x)}I_xP_2S_6(c) + 2xK^+(aq)$$

Electron paramagnetic resonance (EPR) spectroscopy is well suited to the study of the interfacial equilibrium processes involving the exchange of diamagnetic lattice metal ions with paramagnetic intercalate ions. We have employed EPR spectroscopy to examine the dynamic behaviour of the solvent–intercalate complex, as well as the coordination geometry and oxidation state of various intercalate cations. In addition, we have used a combination of EPR and optically detected magnetic resonance (ODMR) spectroscopy to characterize intrinsic defects arising from displacement of the metal cations from their lattice positions to locations in the vWG.

Experimental

Materials

Large single crystals of $Cd_2P_2S_6$ and $Zn_2P_2S_6$ were grown by the iodine transport method [3] in sealed quartz tubes. Chemical microanalysis of individual crystals yielded the following typical compositions: $Cd_2P_2S_6$ (Cd, 44.9 wt.%; P, 12.8 wt.%; S, 42.2 wt.%), $Zn_2P_2S_6$ (Zn, 33.7 wt.%; P, 16.5 wt.%; S, 50.0 wt.%). Cation exchange reactions with transition metal cations were carried out using the procedures described above and discussed more fully in the literature [6].

Instrumental

All EPR measurements were performed on a Brucker 200E-SRCX-band spectrometer using a Brucker TM100 cylindrical cavity with 100 kHz modulation.

The apparatus used for ODMR measurements is similar in design to that described by Cavenett [7] and is capable of operation either in a field-sweep mode or as a frequency-sweep, zero-field

spectrometer operating between 100 MHz and 12 GHz. For field-sweep spectroscopy, a TM_{100} cylindrical microwave cavity was used, resonant at 10.8 GHz, with an unfilled Q of approximately 3000. Zero-field spectra were obtained using a slow-wave helix with a Q of approximately 50.

Discussion

Intralamellar Mn^{2+} ions

EPR spectra were obtained from $Cd_2P_2S_6$ crystals doped with 0.05% (mol/mol) of Mn^{2+} ions during growth by vapor transport. Analysis of the spectra indicate that the manganese ions substitutionally replace lattice Cd^{2+} ions in trigonally distorted octahedral sites [8] to form a $[Mn^{2+}]_{Cd}$ substitutional site. The EPR spectrum of the doped lattice provided a useful reference spectrum for comparison with those of Mn^{2+} ions introduced by cation exchange.

The temperature dependence of the $[Mn^{2+}]_{Cd}$ EPR spectrum revealed a phase transition of the lamellar lattice. Above 300 K, the spectrum is characteristic of a single manganese site (Fig. 2, spectrum A). As the crystal is cooled below about 220 K, all the lines in the spectrum diminish in intensity and a second set of lines appears which gradually becomes dominant (Fig. 2, spectrum B). The fractional intensity of the high temperature spectrum is plotted as a function of temperature in Fig. 2, where the small arrows indicate the direction of temperature change during measurement. The data reveal the presence of a first-order phase transition centred at about 260 K. The high temperature phase yields the spin Hamiltonian parameters $D = -365 \times 10^{-4}\ cm^{-1}$, $E = 6 \times 10^{-4}\ cm^{-1}$, $g_{xx} = 2.006$, $g_{yy} = 2.007$, $g_{zz} = 2.001$. These are consistent with a monoclinic structure. The zero value obtained for the rhombic distortion parameter in the low temperature phase suggests an orthorhombic phase ($D = 353 \times 10^{-4}\ cm^{-1}$, $E = 0$, $g_{xx} = g_{yy} = 2.005$, $g_{zz} = 2.002$. The structure types have been confirmed by X-ray diffraction [8]. Lattice parameter measurements indicated that the structural transition involves a sliding motion of the hexagonally packed sulfur layers aided by the weak interlamellar interactions. The change in monoclinic angle of 17.1° is surprisingly large, especially since this implies a relative displacement of adjacent layers by about 0.2 nm.

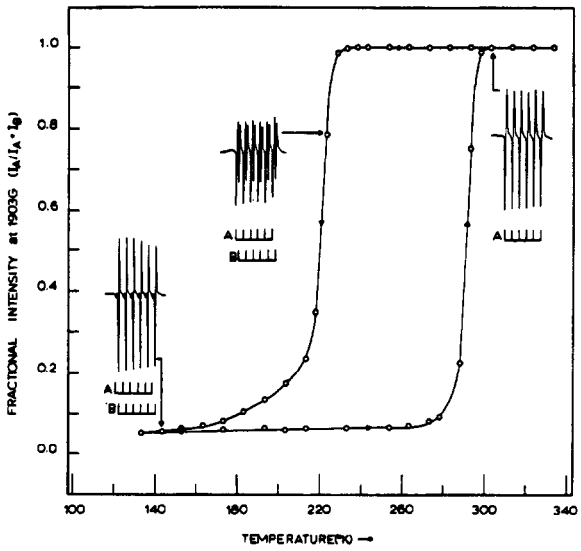

Fig. 2. A first-order phase transition detected by EPR in $Cd_2P_2S_6$.

Interlamellar Mn^{2+} ions

When single crystals of $Cd_2P_2S_6$ are intercalated with Mn^{2+} ions in dilute pyridine-water solution, chemical analysis indicates that Cd^{2+} ions are displaced from the lattice by cation exchange. Pyridine (py) is a moderately strong complexing agent for transition metal cations and assists in the cation exchange process. The EPR spectrum of the intercalated Mn^{2+} ion is shown in Fig. 3 (spectrum a). The spectrum is a superposition of two spectra: a broad background spectrum without resolved hyperfine structure due to $Mn(py)_n(aq)^{2+}$ ($n = 1$, 2) and a six-line hyperfine multiplet spectrum contributed by $Mn(aq)^{2+}$ ions. The EPR spectra of these species have been examined by McGarvey [9]. The intensities of these two spectra indicate the relative amounts of each species pre-

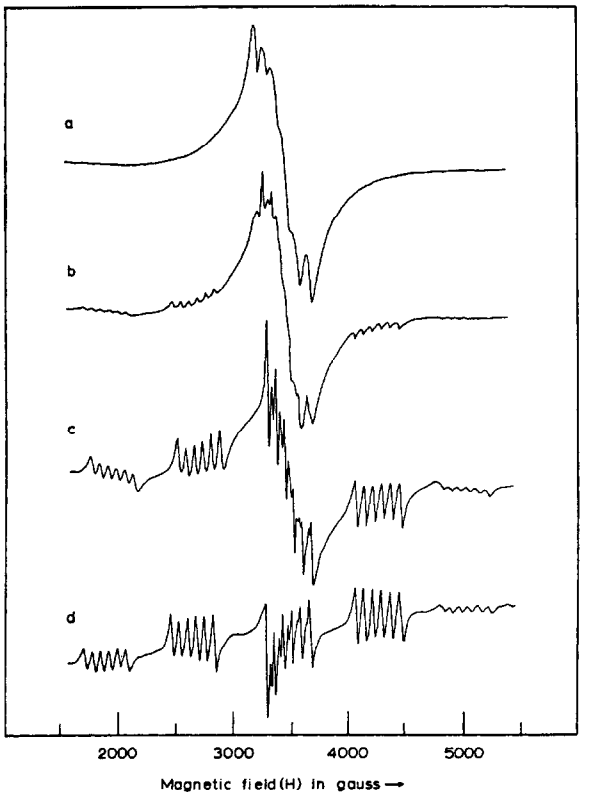

Fig. 3. The EPR spectra of Mn^{2+} cations introduced into $Cd_2P_2S_6$ by cation exchange: spectrum a, complexed with water and pyridine in the vWG; spectra b and c obtained after heating to remove solvent, spectrum d after complete solvent removal.

sent in the interlamellar spaces. The equilibrium for complex formation is substantially shifted in favor of the pyridine complex upon intercalation. McGarvey found that for pyridine concentrations in water of less than about 0.02 M, the ratio $[Mn(py)_n^{2+}]/[Mn(aq)^{2+}]$ equals 90. The EPR spectrum in Fig. 3 (spectrum a) suggests that for complex formation within the van der Waals gap, this ratio is about 3000. The strongly anisotropic structure associated with the $\pm 5/2 \leftrightarrow \pm 3/2$ and $\pm 3/2 \leftrightarrow \pm 1/2$ fine structure transitions, characteristic of Mn^{2+} ions in crystalline lattices, is absent in Fig. 3 spectrum a. This demonstrates that the complexed Mn^{2+} ions are randomly oriented within the interlamellar space.

The intercalated crystal was heated to successively higher temperatures (to 673 K) resulting in thermal deintercalation of the pyridine–water solvent. The increased intensity of the nuclear hyperfine structure associated with the $+1/2 \leftrightarrow -1/2$ fine structure transition (Fig. 3, spectrum b) is caused by a decrease in the amount of pyridine-complexed ion and an increase in the amount of uncomplexed ion. The emergence of the $\pm 5/2 \leftrightarrow \pm 3/2$ and $\pm 3/2 \leftrightarrow \pm 1/2$ anisotropic fine structure transitions (Fig. 3, spectra b and c) is due to increased alignment of the Mn^{2+} ion spin axes. As more pyridine is thermally deintercalated, the EPR spectrum gradually approaches that of the intralamellar $[Mn^{2+}]_{Cd}$ center. Analysis of the EPR spectra indicates that approximately 10–15% of the Mn^{2+} ions intercalated by cation exchange will enter lattice vacancies after heating to 400 °C. These ions are very likely located at the sites vacated by Cd^{2+} ions during the intercalation reaction.

Cation exchange with Co^{2+} ions

An EPR spectrum was obtained at 5 K from a $Cd_2P_2S_6$ crystal doped with 0.05% (mol/mol) Co^{2+} ions during growth by vapor transport. The eight-line hyperfine spectrum with $g_{\parallel} = 4.94$ and $g_{\perp} = 3.99$ is that of substitutional sites, $[Co^{2+}]_{Cd}$, and is observable only below 25 K [10]. The EPR spectra shown in Fig. 4 are obtained at 5 K from crystals exchanged with Co^{2+} ions. The spectra consist of a broad eight-line spectrum ($g_{\parallel} = 5.00$, $g_{\perp} = 3.94$) that increases in intensity at lower temperatures, and a sharp eight-line spectrum ($g_{\parallel} = 4.89$, $g_{\perp} = 3.94$) that disappears below about 5 K.The magnitudes of the g values are similar to the g value for the $[Co^{2+}]_{Cd}$ site. The angle dependence of the EPR spectra indicates that the spin axes are aligned with respect to the crystallographic axes. The ions may be located at either tetrahedral or octahedral interstitial sites within the vWG or at ocahedral cadmium ion vacancies.

In tetrahedral coordination, the crystal field splitting of the ^4F Co^{2+} free-ion ground term yields as $^4A_2$ ground state with the isotropic g value

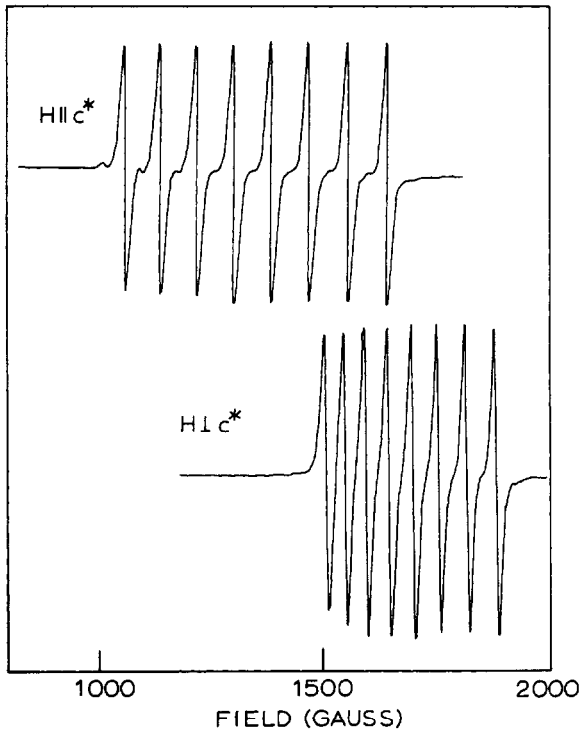

Fig. 4. The EPR spectrum of Co^{2+} cations introduced into $Cd_2P_2S_6$ by cation exchange.

given approximately by

$$g_{iso} = g_e - 8\lambda/10Dq \quad (1)$$

where Dq is the cubic field splitting parameter. Setting the spin–orbit coupling parameter $\lambda = -180\ cm^{-1}$ and $10Dq = 4300\ cm^{-1}$ in Eq. (1) gives $g_{iso} = 2.34$. No resonances are observed with g values close to that expected for tetrahedral coordination. In octahedral coordination the ^4F ground state is split by the crystal field to yield a $^4T_{1g}$ ground state that is further split by spin–orbit coupling into six Kramers doublets. The isotropic g value of the lowest Kramers doublet is given approximately by [11]

$$g_{iso} = (2/3)\alpha + 10/3 - 15\lambda/20Dq \quad (2)$$

For an F state ion $\alpha = 3/2$. If the value of $Dq = 837\ cm^{-1}$ obtained from the electronic spectrum [12] of $Co_2P_2S_6$ is used in Eq. (2), the isotropic g value for octahedrally coordinated Co^{2+} ions is estimated to be 4.49, in good agreement with the average g value observed ($g_{ave} = 4.42$). We conclude that the EPR spectra arise from cations with predominantly octahedral coordination.

The anisotropy of the experimental g values is indicative of a distorted octahedral Co^{2+} ion coordination. The g value anisotropy may be related to the crystal coordination geometry using a simple crystal field model to describe the Co^{2+} ion coordination in terms of three separate parameters: the trigonal angle θ, the familiar cubic field splitting parameter Dq, and the trigonal field splitting parameter Cp [13]. In terms of these parameters, the crystal potential may be written as

$$\begin{aligned} v_{cryst} = {} & 21\sqrt{\pi/5}Cp(3\cos^2\theta - 1)Y_2^0 \\ & + 2\sqrt{\pi}Dq(35\cos^4\theta - 30 + \cos^2\theta + 3)Y_4^0 \\ & + 3\sqrt{35\pi}Dq(\sin^3\theta - \cos\theta)(Y_4^3 - Y_4^{-3} \end{aligned} \quad (3)$$

where Y_l^m are Legendre polynomials of order l. The complete spin Hamiltonian is

$$\mathcal{H} = v_{cryst} + \mathcal{H}_{Zeeman} \quad (4)$$

where $\mathcal{H}_{Zeeman}$ is the magnetic field interaction given by

$$\mathcal{H}_{Zeeman} = \beta \boldsymbol{H}(\boldsymbol{L} + g_e\boldsymbol{S}) + \lambda \boldsymbol{L}\cdot\boldsymbol{S} \quad (5)$$

Using the Hamiltonian of Eq. (5) the ground state g value anisotropy was computed for trigonal angle values $50 \leqslant \theta \leqslant 58$ and $2 \leqslant Cp/Dq \leqslant 12$, corresponding to the full range of physically reasonable values of these parameters. The relationship between the g value anisotropy $\Delta g = (g_\parallel - g_\perp)$ and the parameters θ and Cp/Dq is displayed as a contour plot in Fig. 5.

The results of the calculation demonstrate that when $2 < Cp/Dq < 8$, the sign of the g value anisotropy depends upon whether the trigonal distortion is an elongation or a compression. When $\theta < 54.7$ (trigonal elongation) then $\Delta g < 0$ and when $\theta > 54.7$ (trigonal compression) then $\Delta g > 0$. In fact, this behavior is exhibited by cobalt in a variety of trigonally distorted coordination compounds and crystal lattice sites. When the value of Cp/Dq is

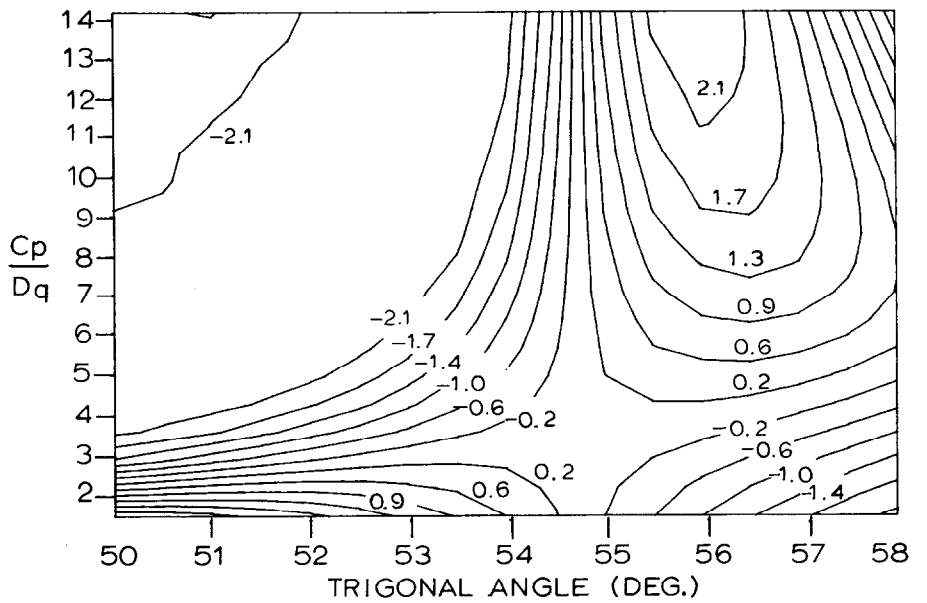

Fig. 5. Behavior of the g value anisotropy as a function of the crystal field parameter Cp/Dq and the trigonal distortion angle θ.

greater than 8 or less than 2, the dependence of the anisotropy upon the distortion angle becomes complex and the anisotropy alone cannot be used to determine the direction of the trigonal distortion.

Both Co^{2+} ion sites in $Cd_2P_2S_6$ exhibit a g value anisotropy $\Delta g \approx +1$, consistent *either* with a trigonal compression *or* a substantial decrease in the Cp/Dq ratio from the value observed in $Co_2P_2S_6$ (about 6) to less than 2. The Cp/Dq ratio is expected to increase when the smaller Co^{2+} cation occupies the larger Cd^{2+} cation vacancy. Therefore we have interpreted the g value anisotropy as indicative of a trigonally compressed Co^{2+} ion sulfur coordination. This interpretation requires the Co^{2+} ion sulfur coordination to be severely distorted from the trigonally elongated coordination of the cation site in the host $Cd_2P_2S_6$ lattice.

Metallocene intercalation

Large molecular species will also intercalate the $M_2P_2S_6$ lattices and the intercalation of metallocenes, $M(cp)_2$ (M = Co, Fe; cp = cyclopentadienyl) has been of particular interest. Both neutral metallocenes and their cations will intercalate many of the $M_2P_2X_6$ lattices [14].

Determination of the oxidation state of the intercalated metallocene is important for an understanding of the intercalation reaction mechanism. It is frequently observed that the metallocene is present as a cation in both MX_2 and $M_2P_2X_6$ lattices. Evidence for this is obtained from examination of the optical spectrum [15], the magnetic susceptibility [16] and the vibrational spectra [17] of the intercalated lattices. Therefore the process of intercalation appears to involve the donation of an electron to the host lattice.

X-band EPR spectra of cobaltocene-intercalated $Cd_2P_2S_6$ obtained at 113 K with $\boldsymbol{H} \| \boldsymbol{c}^*$ and $\boldsymbol{H} \perp \boldsymbol{c}^*$ are illustrated in Fig. 6. When the sample is oriented with $\boldsymbol{H} \perp \boldsymbol{c}^*$, no hyperfine structure is resolved and the resonance signal is an order of magnitude weaker. Since $Co(Cp)_2^+$ is diamagnetic, the EPR spectrum must arise from neutral cobaltocene. The $d^7(\delta^4\sigma^2\pi^1)$ configuration of $Co(cp)_2$ places a single unpaired electron in an antibonding π orbital. The EPR spectrum may be analyzed with the spin Hamiltonian

$$\mathcal{H} = \beta g_{\text{eff}} S_z \boldsymbol{H} + h[A_{\|} S_z I_z + A_{\perp}(S_x I_x + S_y Y_y] \quad (6)$$

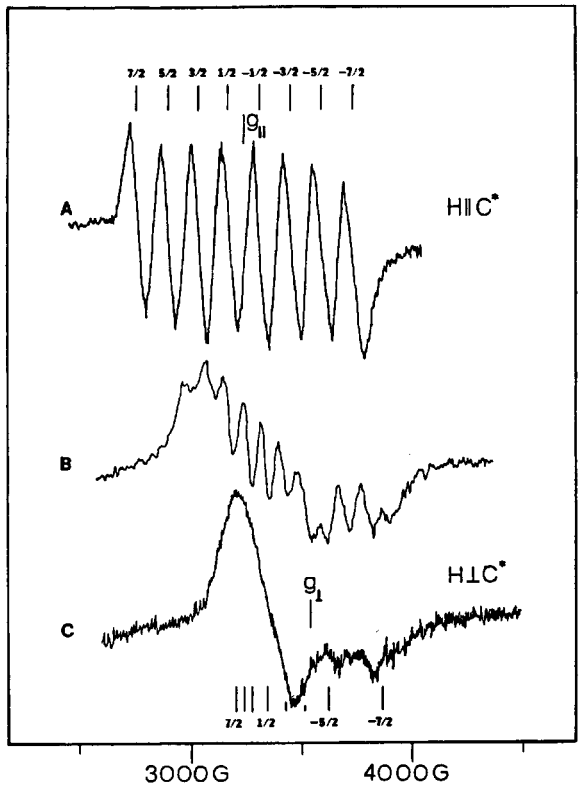

Fig. 6. The EPR spectrum of cobaltocene-intercalated $Cd_2P_2S_6$ obtained with the magnetic field parallel to c^* (spectrum A), at 45 ° to c^*, (spectrum B) and perpendicular to c^* (spectrum C).

where g_{eff} is the effective g tensor given by

$$g_{eff}^2(\theta) = g_{\|}^2 \cos^2\theta + g_{\perp}^2 \sin^2(\theta) \quad (7)$$

The anisotropy in g shifts the EPR spectrum obtained with $\theta = 0°$ ($\boldsymbol{H} \| C_5$) to low field relative to that obtained with $\theta = 90°$ ($\boldsymbol{H} \perp C_5$). The cobalt nuclear spin ($I_{co} = 7/2$) results in the splitting of the single $S = 1/2$ electron spin transition into a nuclear hyperfine octet. The hyperfine structure is expected to be well resolved in the $g_{\|}$ spectrum, and poorly resolved in the $g_{\perp}$ spectrum owing to the large anisotropy ($A_{\|} \gg A_{\perp}$) of the nuclear hyperfine coupling tensor [18]. The well-resolved, low field octet obtained with $\boldsymbol{H} \| c^*$, arises from netural $Co(cp)_2$ with $C_5 \| \boldsymbol{H}$. Therefore the EPR spectrum

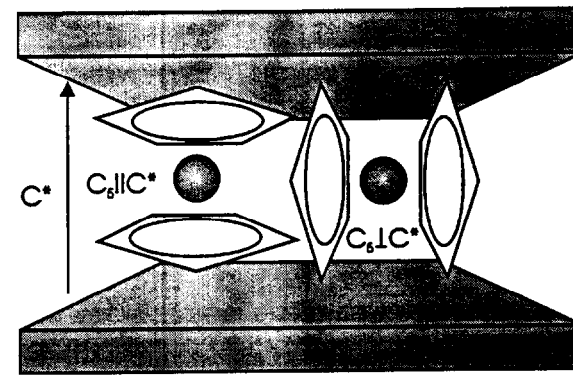

Fig. 7. Proposed orientations of intercalated metallocenes.

Analysis of the spectra yields $g_{\|} = 2.00$ and $g_{\perp} = 1.96$. These values are considerably greater than observed for $Co(cp)_2$ in a variety of other crystal lattices and rare gas matrices. In general, as the axial symmetry of the metallocene is decreased, both $g_{\|}$ and $g_{\perp}$ increase toward the value $g_e \approx 2$. The relatively large values obtained for $g_{\|}$ and $g_{\perp}$ indicate a decrease in molecular axial symmetry within the vWG that may occur as a result of either strong intercalated–lattice or intermolecular interactions.

Cation vacancies

Metal vacancy and interstitital defects are common in transition metal chalcogenide lattices. $M_2P_2S_6$ lattices are particularly prone to the formation of these defects because of the high liability of the transition metal and the accessibility of the extended interstital space in the vWG. Octahedral holes in the vWG can accommodate the transition metal interstitials with relatively little energy penalty. There is substantial physical evidence to support the existence of metal vacancies in the $M_2P_2S_6$ lattice. Splitting of the PS_3 IR deformation mode has been attributed to the presence of metal vacancies [19], and the characteristic orange-red photoluminescence (PL) spectrum of the $M_2P_2S_6$ lattices is associated with the presence of lattice

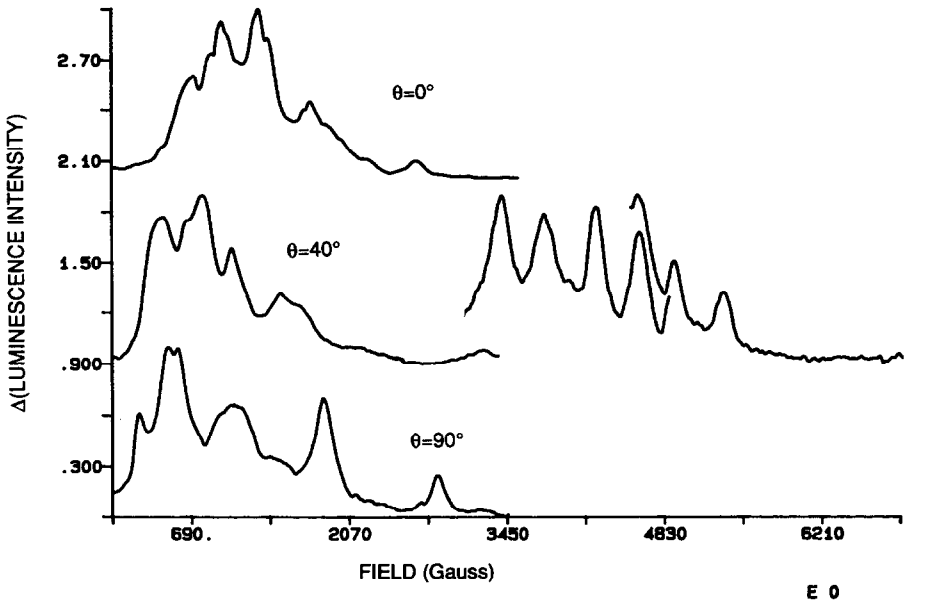

Fig. 8. ODMR spectra of $Zn_2P_2S_6$.

and vacancy defects. However, large concentrations are observed in quench-cooled crystals, suggesting a tendency of the metal to establish an equilibrium between regular lattice sites and vWG sites at elevated temperatures.

A neutral metal interstitial in the vWG, which we designate $[M]_{vWG}$, is the electron donor and a neutral metal vacancy $[V]_M$ is a double electron acceptor. Since the cation exchange process removes lattice metal as the cation M^{2+} we expect that the lattice contains predominately doubly charged vacancy acceptors $[V^{2-}]_M$, although $[V^-]_M$ and $[M^+]_{vWG}$ centers may also be present. However, the paramagnetic $[V^-]$ and $[M^+]$ centers cannot be present in large concentrations, (below $10^{11}\,cm^{-3}$) since they are not detected by EPR.

Isolated $[V^{2-}]_M$, $[V^0]_M$, $[M]_{vWG}$ and $[M^{2+}]_{vWG}$ centers are diamagnetic in their ground states, but can be detected and characterized by magnetic resonance in paramagnetic photoexcited states using the technique of ODMR. The methods and principles of ODMR have been described in several excellent reviews [7]. Photoexcitation of these lattice donor and acceptor centers can produce a variety of photoexcited states. We focus only on the processes believed responsible for the photoinduced paramagnetism observed in $Zn_2P_2S_6$ and $Cd_2P_2S_6$. In particular, since the PL spectrum is essentially independent of the interstital cation's chemical identity, oxidation state and concentration, it is believed that the vacancies and interstitials are not strongly coupled and can be described independently.

$Zn_2P_2S_6$ ODMR

The native zinc compound exhibits the strong ODMR spectra illustrated in Fig. 8. These were obtained by monitoring the 2.390 eV vacancy luminescence. It is also possible to observe a strong ODMR signal in zero field at about 10.7 GHz (Fig. 9). The observation of a zero-field splitting indicates that the ODMR signal arises from a spin triplet that can be described by the following spin Hamiltonian:

$$\mathscr{H}_T = \beta g \boldsymbol{B}\cdot\boldsymbol{S} + D[S_Z^2 - (1/3)S(S+1)] + E(S_x^2 - S_y^2) + \boldsymbol{I}\cdot\boldsymbol{A}\cdot\boldsymbol{S} \quad (8)$$

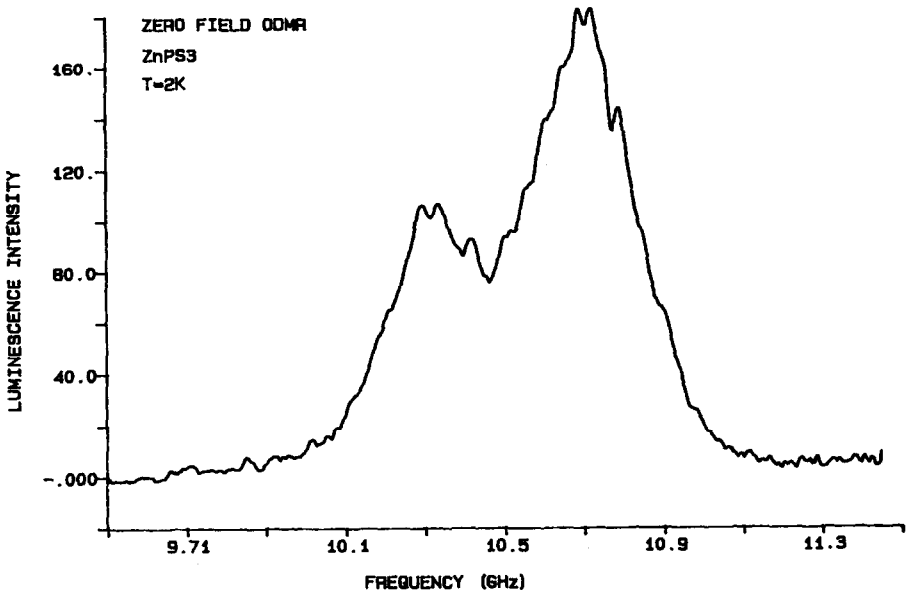

Fig. 9. The zero-field ODMR spectrum of $Zn_2P_2S_6$.

where the notation used is conventional [20].

The angle dependence of the ODMR spectrum reveals that it consists of a superposition of resonances from several crystallographically equivalent but magnetically inequivalent centers. The multiplicity of lines and the angular dependence of the spectrum can be accurately reproduced using the Hamiltonian of Eq. (8) if the principal magnetic axis of the center is aligned about 70° to c^* and allowed to adopt any one of three equivalent positions interrelated by a threefold rotation about c^*. When $H \| c^*$ ($\theta = 0$), all three positions are magnetically equivalent and a relatively simple ODMR spectrum is obtained; when H is inclined to c^*, the sites are resolved into magnetically equivalent sets that give rise to the distinctive low field and high field ODMR spectra.

The spectrum also exhibits a quartet hyperfine pattern due to coupling with the nuclear spin of a single phosphorus atom ($I = 1/2$). The complex hyperfine pattern is due to the presence of both allowed ($\Delta m_I = 0$) and forbidden ($\Delta m_I = \pm 1$) transitions. The nominally forbidden hyperfine transitions are observed with considerable intensity when the field is oblique to the spin axes of the site. The effect is enhanced because the zero-field splitting is comparable to the microwave frequency and the nuclear spin is only weakly quantized with respect to the external field. The best agreement with the experimental spectrum was obtained with an isotropic g value of 1.8 and $D = 15.7$ GHz, $E = 5.3$ GHz, $A_{xx} = 2$ GHz, $A_{yy} = 2$ GHz and $A_{zz} = 3$ GHz.

The ODMR spectrum appears to arise from the triplet state of an isolated, neutral zinc vacancy center, $[V]_M$ which is generated by irradiation of the predominant $[V^{2-}]_M$ center at low temperatures. The neural vacancy is formed when a $[V^{2-}]_M$ center traps two photogenerated holes at the sulfur atoms that form the coordination environment of the zinc vacancy. The isolated vacancy may be described using a molecular orbital formalism to construct six symmetry-adapted vacancy orbitals from six orbitals of the coordinating sulfur atoms. A similar description of *tetrahedrally* coordinated zinc vacancies was presented by Rong et al. [21] for the $[V^-]_M$ center in ZnSe and tetrahedral centers have also been reported in CdS, ZnO and BeO [22]. For example, Galland and Herve [23] report a triplet EPR spectrum associated with the

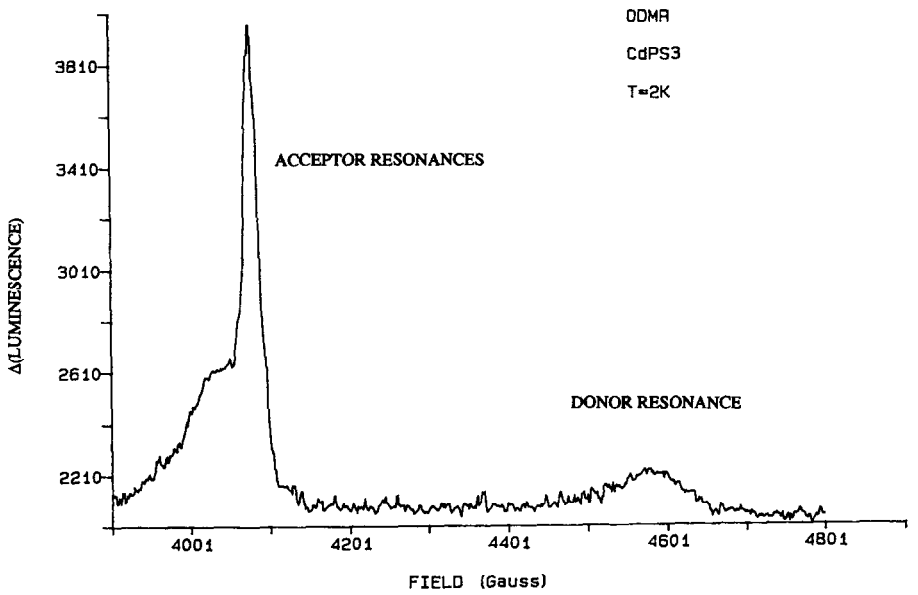

Fig. 10. ODMR spectra of $Cd_2P_2S_6$ isolated donor and acceptor sites.

neutral charge state of the zinc vacancy in ZnO under UV illumination at 90 K. The centers are composed of two holes trapped on two non-axial oxygen atoms surrounding the vacancy. Poppl and Volkl [24] have also observed a triplet state of the neutral vacancy in sintered ZnO samples under illumination with a mercury arc lamp at 7 K.

$Cd_2P_2S_6$ ODMR

ODMR signals could not be detected from $Cd_2P_2S_6$ unless vacancies had been induced by cation exchange. The ODMR spectrum is detected via the 1.66 eV vacancy PL band that is induced by the creation of cation vacancies. The ODMR spectrum, shown in Fig. 10, has an appearance that is characteristic of isolated, $S = 1/2$ donors and acceptors in many II–VI semiconductors.

Since the donor–acceptor coupling is weak compared with the Zeeman interaction, the magnetic interactions can be described by the following Hamiltonian:

$$\mathscr{H} \approx \beta g_A \boldsymbol{H}\cdot\boldsymbol{S}_A + \beta g_D \boldsymbol{H}\cdot\boldsymbol{S}_D \qquad (9)$$

A sharp, strong, low field resonance at $g_A = 1.916 \pm 0.005$ is overlapped by a weaker, broader resonance at $g_D = 1.904 \pm 0.005$. The low field resonances identify two different acceptor centers in the $Cd_2P_2S_6$ lattice. For both resonances, the g value is isotropic. This is fairly typical behaviour for electrons localized at cation vacancies in II–VI lattices. For example, g values associated with zinc vacancy centers (A centers) in ZnS exhibit both isotropic and weakly axial g values in the range 2.00 ± 0.051 [25]. The isotropic g value may be due to the electron hopping between equivalent sulfur atoms in a nearly octahedral arrangement about the cation vacancy. The high field donor resonance at $g_D = 1.694 \pm 0.005$ is also nearly isotropic, but broader and much weaker than the acceptor resonance. This behavior is consistent with that expected for a shallow donor. Because of the proximity of the donor to the conduction band, it is relatively more delocalized and yields a weaker ODMR signal, frequently without resolved nuclear hyperfine structure. The electron donors may be interstitial metal cations; however, we cannot unambiguously identify the donor defect in the absence of resolved hyperfine structure.

Conclusion

EPR and ODMR techniques have proved to be of considerable utility for the study of the complex, solid state cation exchange process exhibited by $M_2P_2S_6$ materials. These studies reveal that cations may occupy octahedral sites in the interlamellar vWG and at intralamellar cation vacancies. The distribution between sites depends upon the choice of solvent and metal cation. Larger paramagnetic species, such as the metallocenes, reside in the vWG and may be relatively well ordered.

ODMR measurements demonstrate the presence of both intrinsic and cation-exchange-induced lattice vacancies in $M_2P_2S_6$ lattices. The vacancies act as acceptor sites and probably doubly ionized.

Acknowledgments

A.H.F. would like to acknowledge support from the National Science Foundation (DMR 8 818 371). International collaboration was greatly assisted by awards from the NATO Research Programme to A.H.F. and R.C., and the US–Israel Binational Science Foundation to E.L. and A.H.F. (89-00316).

References

1 R. Schöllhorn, Physica, 99B (1980) 89.
2 R. Brec, Solid State Ionics, 22 (1986) 3.
3 C.E. Byvik, B. Reichman and D.W. Coleman, J. Electrochem. Soc., 237 (1982).
4 V.W. Klingen, R. Ott and H. Hahn, Z. Anorg. Allg. Chem., 396 (1973) 271.
5 R. Clement, J. Chem. Soc., Chem. Commun., (1980) 647.
R. Clement, J. Am. Chem. Soc., 103 (1981) 6998.
6 R. Clement, O. Garnier and J. Jegoudez, J. Inorg. Chem., 25 (1986) 1404.
7 B.C. Cavenett, Adv. Phys., 30 (1981) 475.
8 E. Lifshitz and A.H. Francis, J. Phys. Chem., 86 (1982) 4714.
E. Lifshitz, A.H. Francis and R. Clarke, Solid State Commun., 45 (1983) 273.
9 B.R. McGarvey, J. Phys. Chem., 61 (1957) 1232.
10 G.T. Long and D.A. Cleary, J. Phys. Condens. Mater., 2 (1990) 4747.
11 A. Abragam and M.H.L. Pryce, Proc. R. Soc. London, Ser. A, 173 (1951) 206.
12 N. Nagasundaram and A.H. Francis, J. Phys. Chem. Solids, 50 (1989) 163.
13 M. Gerloch and R.C. Slade, Ligand-Field Parameters, Cambridge University Press, London, 1973.
14 Y. Mathey, R. Clement, C. Sourisseau and G. Lucazeau, Inorg. Chem., 19 (1980) 2773.
D. Cleary and A.H. Francis, J. Phys. Chem., 89 (1985) 97.
R. Clement, O. Garnier and Y. Mathey, Nouv. J. Chim., 6 (1982) 13.
R. Clement, O. Garnier, H. Mercier, J.-P. Audiere, A. Michalowicz, B. Rousseau and R. Setton, J. Chem. Soc., Chem. Commun., (1984) 1354.
15 J.P. Audiere, R. Clement, Y. Mathey and C. Mazieres, Physica B + C, 99 (1980) 133.
R. Clement, O. Garnier and Y. Mathey, Nouv. J. Chim., 6 (1982) 13.
16 R. Clement, J. Girerd and I. Morgenstern-Badarau, Inorg. Chem., 19 (1980) 2852.
17 C. Sourisseau, J.P. Forgerit and Y. Mathey, J. Phys. Chem. Solids, 44 (1983) 119.
Y. Mathey, R. Clement, C. Sourisseau and G. Lucazeau, Inorg. Chem., 19 (1980) 2773.
18 J.H. Ammeter, Jr., and J.D. Swalen, J. Chem. Phys., 57 (1972) 678.
19 P. Lacroix, J.P. Audiere and R. Clement, J. Chem. Soc., Chem. Commun., 536 (1989).
20 J.E. Wertz and J.R. Bolton, Electron Spin Resonance, McGraw–Hill, New York, 1972, p. 223.
21 F. Rong, W.A. Barry, J.F. Donegan and G.D. Watkins, Phys. Rev. B, 37 (1988) 4329.
22 R.K. Watts, Point Defects in Crystals, Wiley, New York, 1977, p. 250.
23 D. Galland and A. Herve, Phys. Lett. A, 33 (1970) 1.
24 A. Poppl and G. Volkl, Phys. Status Solidi A, 125 (1991) 571.
25 J.E. Nicholls, J.J. Davies, B.C. Cavenett, J.R. James and D.J. Dunstan, J. Phys. C, 12 (1979) 361, and references cited therein.